

# Growth Characteristics of Metallic Iron Particles in the Direct Reduction of Nickel Slag



XIAOMING LI, YI LI, XINYI ZHANG, ZHENYU WEN, and XIANGDONG XING

Coal-based direct reduction of nickel slag and magnetic separation of iron are effective methods of secondary resource utilization. The growth characteristics of metallic iron particles in this process are of great significance for subsequent grinding and magnetic separation process. The nickel slag is mixed with coal powder and other additives in a certain proportion, and then subjected to a direct reduction experiment in a high-temperature furnace. Chemical analysis is made to obtain the components of the direct reduction product. The microstructure of the metallic iron particles in the reduction product was studied and the curves of average diameter change and the cumulative diameter percentage of the iron particles are obtained in the reduction process. The results show that the coal-based direct reduction technology can effectively reduce the iron oxides in the nickel slag, and the degree of metallization of the product can reach 91.89 pct. When the reduction time is increased from 10 to 60 minutes, the maximum size of metallic iron particles increases from 13 to 135  $\mu\text{m}$ . The control mechanism of iron particle growth is complicated, and the process is divided into two stages. The growth kinetic parameters (kinetics index, activation energy, and pre-exponential factor) in the two stages are 0.4697, 249.04  $\text{kJ mol}^{-1}$ ,  $3.81 \times 10^8$  and 1.0774, 92.93  $\text{kJ mol}^{-1}$ , 217.30, respectively. The growth model of metallic iron particles in the direct reduction of nickel slag is also constructed in the paper.

<https://doi.org/10.1007/s11663-020-01799-8>

© The Minerals, Metals & Materials Society and ASM International 2020

## I. INTRODUCTION

THE use of direct reduction iron in ironmaking helps to reduce its dependence on coal resources, cut down energy consumption, and improve the quality of steel products. The raw material for producing direct reduction iron may be various iron-containing resources. With the growing shortage of high-grade resources and the increase of secondary iron resources, using coal-based reduction–magnetic separation process to produce metallic iron from low-grade complex ore<sup>[1,2]</sup> or smelting slag is of great importance. It is an effective measure to make up for ironmaking raw materials, effectively utilize secondary resources, and solve environmental problems.<sup>[3,4]</sup>

As solid waste is produced by nickel smelting industries,<sup>[5]</sup> nickel slag contains large amounts of recoverable and valuable metals. When dumped in open air, it not only occupies vast areas of land, but also pollutes the surrounding environment. There is a growing concern over the utilization of nickel slag. Based on the direct reduction–magnetic separation technology, the recovery of valuable elements from nickel slag is not only a requirement for secondary resource utilization, but also has environmental, economic, and social benefits. Wang *et al.*<sup>[6,7]</sup> studied the effects of additives and base on the deep reduction recovery rate of nickel slag pellets. Gao *et al.*<sup>[8,9]</sup> investigated the formation and growth behavior of metallic iron particles during the direct reduction of refractory iron ore. Pan *et al.*<sup>[10]</sup> researched the effect of time, temperature, and amount of coal on magnetic separation and reduction of nickel slag. Kinetic studies on nickel slag by Guo *et al.*<sup>[11]</sup> and thermodynamics on laterite ore by Luo *et al.*<sup>[12]</sup> showed that the size of metallic iron particles varies greatly in the reduction process in which the larger the particle size, the easier it is to separate it from the slag and the better the magnetic separation effect. Therefore, the key to achieving more effective reduction and increasing the recovery rate of magnetic separation is to conduct in-depth research on

---

XIAOMING LI and XIANGDONG XING are with the School of Metallurgical Engineering, Xi'an University of Architecture and Technology, Xi'an 710055, P.R. China and also with the Research Center of Metallurgical Engineering and Technology of Shaanxi, Xi'an University of Architecture and Technology, Xi'an 710055, P.R. China. Contact e-mails: xml88@126.com, xaxingxiangdong@163.com YI LI, XINYI ZHANG, and ZHENYU WEN are with the School of Metallurgical Engineering, Xi'an University of Architecture and Technology.

Manuscript submitted June 3, 2019.

Article published online February 28, 2020.

**Table I. Chemical Components of Nickel Slag (Mass Percent)**

TFe	FeO	SiO <sub>2</sub>	MgO	CaO	Ni	Cu	Co	S
39.40	49.68	32.50	9.70	1.20	0.455	0.338	0.144	0.868

the formation of iron grains, the aggregation and growth mechanism of iron particles, and the process control during the direct reduction of nickel slag.

Through high-temperature reduction experiments, the paper studies the effects of reduction time, temperature, and basicity (CaO/SiO<sub>2</sub>) on the coal-based reduction of nickel slag. With the help of scanning electron microscopy (SEM), the growth of iron particles during the reduction process is observed. The Image-pro Plus (IPP) software is used to determine the iron particle size, and the growth pattern of metallic iron particles during the coal-based direct reduction process of the nickel slag is clarified. Based on the classical grain growth theory, the growth kinetics of metallic iron particles is calculated.

## II. EXPERIMENT

### A. Raw Materials

The nickel slag in the experiment comes from Jinchuan Group Co., Ltd., China. Table I gives the main chemical components, in which the total iron content is 39.40 pct. The results of phase analysis of the nickel slag are shown in Figure 1, with the main phase components being Fe<sub>2</sub>SiO<sub>4</sub>, Mg<sub>2</sub>SiO<sub>4</sub>, and FeNiS<sub>2</sub>.

The reductant coal used in the experiment was from Panzhihua Iron & Steel in Sichuan Province, China. The proximate analysis of the reducing agent coal powder is shown in Table II. High in fixed carbon content and low in harmful impurities such as phosphorus and sulfur, coal powder is ideal as a reducing agent. In this paper, as volatile matter in coal slightly influenced reduction, coal was regarded as a whole in each experiment, and the effect of volatile on reduction was not considered in isolation. Shown in Table III is the chemical components of the coal ash, which is mainly composed of SiO<sub>2</sub> and Al<sub>2</sub>O<sub>3</sub>, followed by Fe<sub>2</sub>O<sub>3</sub>, CaO, and MgO.

### B. Experiment Process

The nickel slag was dried at 393 K for 5 hours and then pulverized with a roll crusher to be particles of smaller than 75 μm. The reducing agent coal was pulverized to be particles of smaller than 75 μm. The properly sized nickel slag, reducing agent, binder (hydroxymethyl sodium), and water were mixed at the mass ratio of 1:0.15:0.01:0.08 and pressed into blocks, each weighing about 5 g. The blocks were then put into a corundum crucible for use.

The reduction process was carried out in a vertical high-temperature furnace. Before the experiment, argon was passed to wash the furnace for a long time. Throughout the experiment, the furnace was filled with

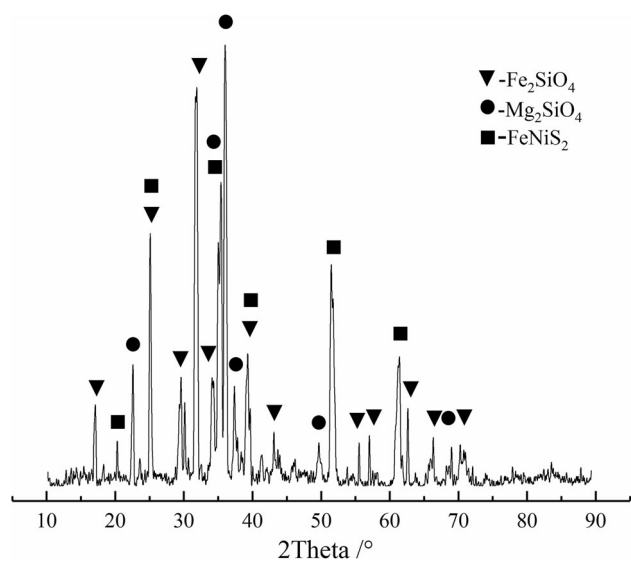


Fig. 1—X-ray diffraction patterns of nickel slag sample.

argon at a flow rate of 20 mL/min to guarantee the oxygen-free environment in the furnace. When the preheating of the shaft furnace was raised to the required temperature (1373 K, 1423 K, 1473 K, 1523 K) at a rate of 20 K/min, the crucible was quickly put into the furnace. At the preset reduction time (10, 20, 30, 40, 50, 60 minutes), the reduced sample was taken out quickly and was covered with pulverized coal to isolate it from air, with the reduced product naturally cooled to room temperature for use.

The cooled reduction product was ground to particles of less than 75 μm and separated into two parts. One was for composition analysis chemically and the other for analysis of morphology and microstructure with an SSX-550 scanning electron microscope.

### C. Analysis and Characterization

The degree of metallization of the reduction product is calculated by Eq. [1], where TFe and MFe are the total iron content and the metallic iron content, respectively.

$$DM = \frac{MFe}{TFe} \cdot 100 \text{ Pct} \quad [1]$$

The growth of metallic iron particles in the reduction product is analyzed by SEM. The sample preparation steps are as follows: First, the reduction product is embedded in resin and polished. Then, the polished sample is dried in an oven at 393 K for 8 hours. After it is completely dried, it is taken out and placed on the

**Table II. Proximate Analysis of the Coal Powder (Mass Percent)**

Water Content	Ash Content	Volatile Content	Fixed Carbon	P	S
0.21	12.72	9.80	77.27	0.005	0.027

conductive paste and then gold is sprayed on its surface. The SEM spectrum is shown in Figure 2(a), in which the bright white color represents metallic iron particles (it is presumed that the iron phase in the actual product is close to a spherical shape). The IPP software is used to process Figure 2(a) and obtain the binary image, as shown in Figure 2(b). Around 1000 to 2000 metallic iron particles obtained under the same experimental conditions are collected and analyzed in order to obtain their growth characteristics.

The circumference of the iron particles in the binary image can be analyzed directly by the IPP software, and what is obtained is the plane size. The relationship between the diameter  $d$  of the actual iron particles and the measured value  $L$  can be expressed by Eq. [2].

$$d = \frac{L}{\pi}, \quad [2]$$

where  $d$  is the spherical diameter ( $\mu\text{m}$ ) of metallic iron particles, and  $L$  is the measured planar perimeter ( $\mu\text{m}$ ), as shown in Figure 2(b). The average diameter of the iron particles can be expressed as

$$\bar{d} = \frac{\sum_{i=1}^N d_i}{N}, \quad [3]$$

where  $\bar{d}$  is the average diameter ( $\mu\text{m}$ ) of the metallic iron particles, and  $N$  is the number of particles.

The metallic iron particle size is calculated by Eq. [4], and a characteristic curve of the cumulative percentage of the particle size is obtained.<sup>[13]</sup>

$$Y(d) = \frac{\sum_{i=d_{\min}}^d \left[ (d/2)^3 \times n_i \right]}{\sum_{i=d_{\min}}^{d_{\max}} \left[ (d/2)^3 \times n_i \right]} \times 100 \text{ Pct}, \quad [4]$$

where  $Y$  is the cumulative percentage of iron particles with a diameter smaller than  $d$ ,  $d$  is the particle diameter ( $\mu\text{m}$ ),  $n$  is the total number of iron particles with a diameter of  $d$ ,  $d_{\max}$  is the maximum diameter ( $\mu\text{m}$ ) of the metallic iron particles, and  $d_{\min}$  is the minimum diameter ( $\mu\text{m}$ ) of the particles.

### III. RESULTS AND DISCUSSION

#### A. Growth Characteristics of Metallic Iron Particles

The SEM spectrum of the reduction product is shown in Figure 3, in which the nearly circular bright part represents metallic iron particles, while the gray area is the slag phase. The enrichment and growth of the metal

**Table III. Chemical Components of the Coal Ash (Mass Percent)**

SiO <sub>2</sub>	Al <sub>2</sub> O <sub>3</sub>	CaO	MgO	TiO <sub>2</sub>	Na <sub>2</sub> O	K <sub>2</sub> O	Fe <sub>2</sub> O <sub>3</sub>
28.4	15.8	2.6	2.5	1.4	0.2	1.9	4.0

iron phase is conducive to the separation between iron and slag. The reduction product detected by energy disperse spectroscopy consists mainly of Fe, Si, O, Mg, S, with S concentrated in the vicinity of the iron phase after reduction.

The variation of the average size of the metallic iron particles in the reduction product of the nickel slag with the reduction time and temperature is shown in Figure 4. The reduction time and temperature have a significant influence on the size of the metallic iron particles and are the main contributors to the growth of the iron particles. With the increase of reduction time, the average diameter of metallic iron particles at different reduction temperatures shows a similar upward trend. At a temperature of 1373 K, when the reduction time is increased from 10 to 60 minutes, the average size of the iron particles increases from 0.9 to 3.7  $\mu\text{m}$ . At a temperature 1523 K, the average size of the iron particles increases from 3.5 to 10.3  $\mu\text{m}$ . It can be speculated that the particle size will continue to increase as time passes and the temperature rises.

#### B. Degree of Metallization of Nickel Slag Direct Reduction

The relationship between the degree of metallization of the reduction product and the reduction time and temperature is shown in Figure 5. At a certain temperature, as the reduction time goes on, the degree of metallization increases first, and then tends to stabilize. The reduction process can be divided into two stages—growth and stabilization—with 40 minutes as the cut-off point. In the growth stage, the iron oxide in the nickel slag is reduced massively, so that the degree of metallization rises rapidly. In the stabilization stage, the reduction reaction is basically completed. It is time for the aggregation and growth of metallic iron particles so that the degree of metallization remains basically unchanged. Meanwhile, the temperature has a significant effect on the degree of metallization. When the

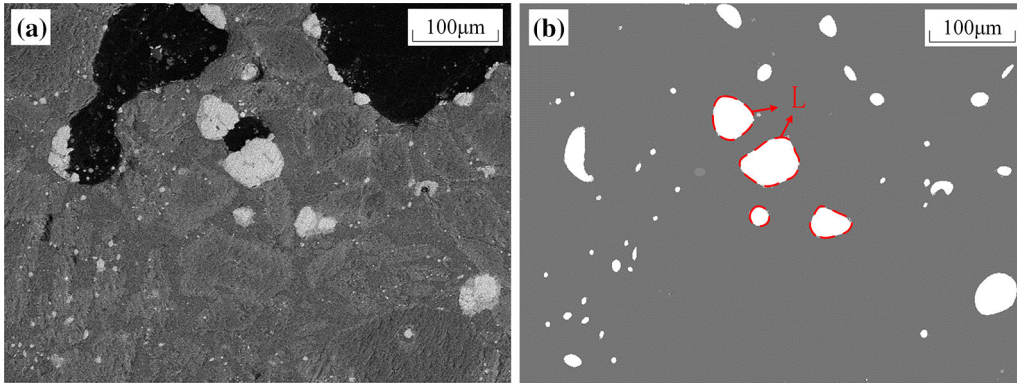


Fig. 2—Scanning electron micrographs of the reduction product of the nickel slag: (a) original image, (b) binary image.

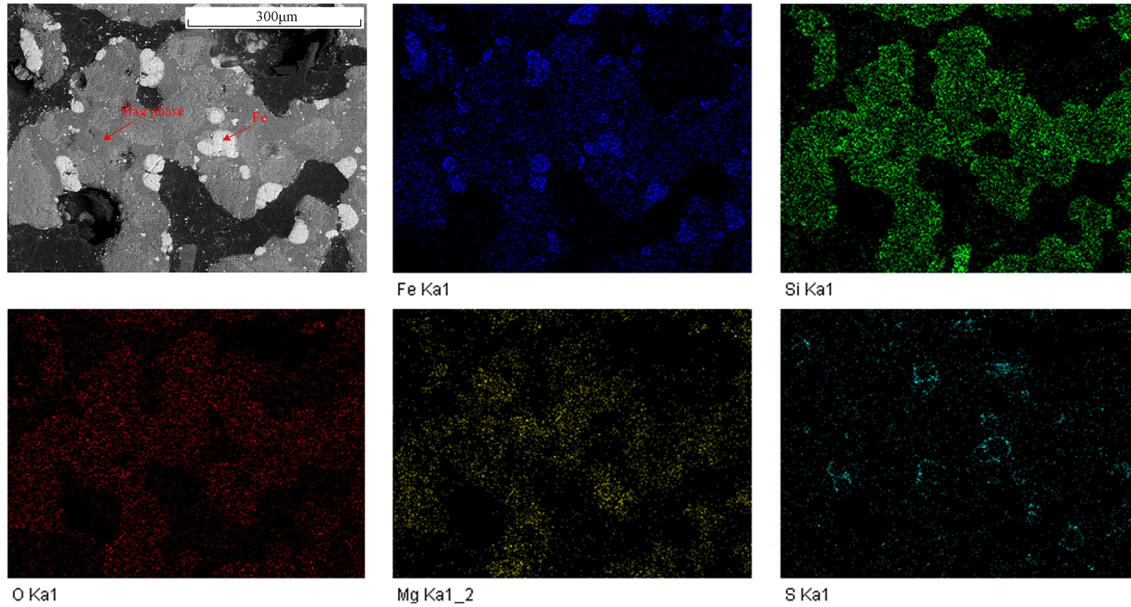
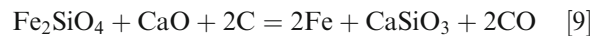
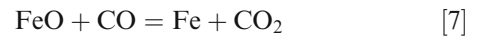
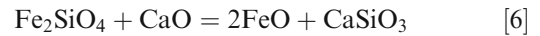
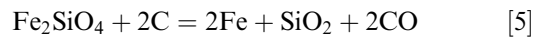


Fig. 3—Scanning electron micrographs of the nickel slag reduced at 1423 K for 30 min.

reduction time is 15 minutes, the degree of metallization corresponding to a temperature rise from 1373 K to 1523 K increases from 8.31 to 20.87 pct. When the reduction time is 60 minutes, the degree of metallization increases from 62.34 to 91.89 pct, corresponding to a temperature rise from 1373 K to 1523 K.

The growth mechanism of metallic iron particles in the coal-based reduction of nickel slag can be described in Figure 6. In the initial stage of reduction, due to relatively low temperature and small reduction rate, there is not much change in the physical structure and size of the nickel slag and the reducing agent coal. As the temperature rises, the iron silicate in the nickel slag begins to dissociate and reacts as follows<sup>[10]</sup>:





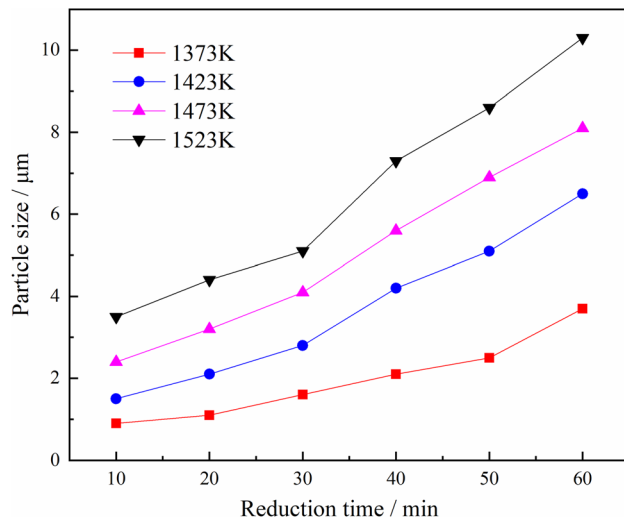


Fig. 4—Effect of reduction time and temperature on the average size of iron particles.

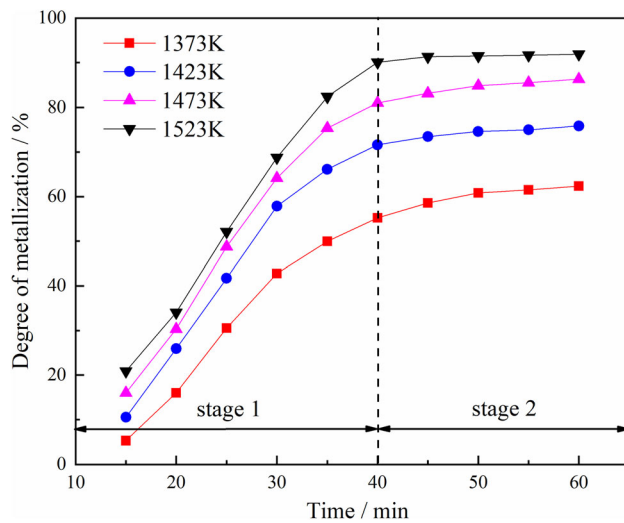
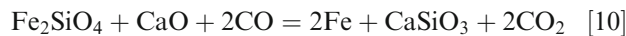


Fig. 5—Effect of reduction time and temperature on the degree of metallization of nickel slag direct reduction.



When the temperature rises to 1073 K, the coal undergoes a reduction reaction with the dissociated fayalite, generating small metallic iron particles, as shown in Eq. [5]. The high experimental temperature intensifies the carbon diffusion in the reaction process, and the method of pressing blocks is adopted to make the contact between solid materials closer, which is conducive to the reduction. The formation of metallic iron particles within the nickel slag indicates that the gas–solid reaction took place in the reaction. The substitution of FeO by CaO in the fayalite resulted in the reaction of FeO and C/CO, which resulted in the formation of metallic iron particles. The corresponding equations were Eqs. [6] through [8], and the total

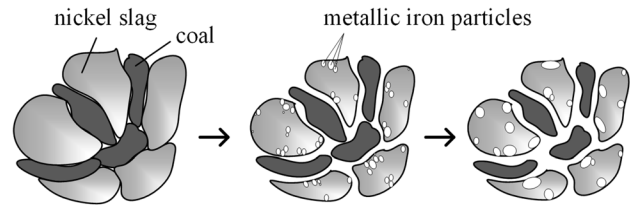


Fig. 6—Growth mechanism of metallic iron particles in the coal-based direct reduction of nickel slag.

reaction would be Eqs. [9] and [10]. All these reactions occur in the system. When the temperature rises to 1273 K to 1473 K, as the reduction reaction proceeds, more and more iron particles gradually form inward from the edge of the reactant, and the space between particles increases. With the decrease of the reducing agent coal, the reaction speeds up rapidly and the reactant shrinks considerably, causing the grain porosity to increase rapidly. The number of metallic iron particles increases gradually and accumulates into a region. According to the principle of minimum free energy, the reduced metallic iron grows into spherical particles, which are embedded in the slag phase. It gradually moves from the central part of the slag phase to the surface before being integrated into large particles. At the end of the reaction, the final product stabilizes in the form of metallic iron. The reduction time and temperature have a significant effect on the growth of metallic particles, and the reduction temperature is positively correlated with the reduction rate within a certain range.<sup>[14]</sup> Raising the reduction temperature not only increases the reduction rate of nickel slag, but improves the diffusion rate of the metallic iron phase as well. When the reduction time is fixed, with the rise of temperature, the raw materials involved in the reduction reaction become more active and the carbon pellet reaction is intense. As the reduction time and temperature increase, the number of large-size metal particles increases, indicating that the average size of the metallic iron particles increases gradually.

### C. Factors Affecting the Growth of Metallic Iron Particles

#### 1. Effect of time on iron particle size distribution

The morphology of the reduction product of nickel slag at 1473 K and of different durations is shown in Figure 7. When the reduction time is less than 20 minutes, the metallic iron particles in the sample are in the nucleation stage, as shown in Figures 7(a) and (b). In this stage, due to the weak diffusion ability of the metallic iron particles and high growth resistance, the maximum particle size is about 12 μm. As the reduction continues, the size of the particles increases rapidly, as shown in Figures 7(c) through (f). From the thermodynamics<sup>[15]</sup> perspective of metallic iron particle nucleation, small-size grains less than the critical radius gradually disappear during the growth stage and iron moves around the nucleus to form larger-size iron grains. From the results of kinetic analysis, 30 minutes of reduction was used as the boundary of two kinetic

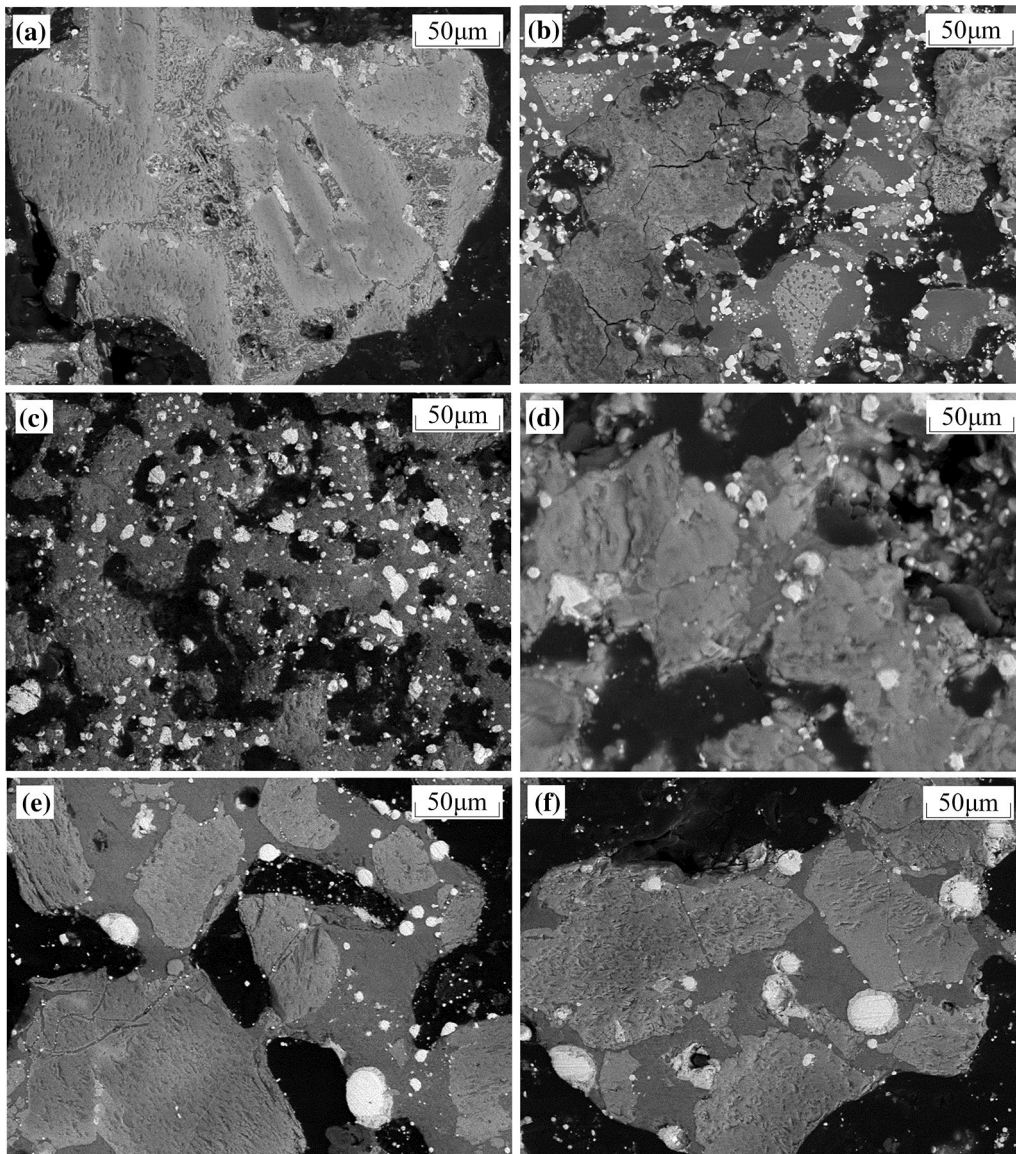


Fig. 7—Scanning electron micrographs of the nickel slag reduced at 1473 K for (a) 10 min, (b) 20 min, (c) 30 min, (d) 40 min, (e) 50 min, (f) 60 min.

stages. Before 30 minutes of reduction, the main process was the reduction of nickel slag to produce iron, and a nucleus has been formed by this time. The average size of the grains around the nucleus is still small. Metallic iron particles have a small specific surface area, high surface activity, and low resistance of particle diffusion and migration.<sup>[16,17]</sup> Therefore, iron in the fine grains around the crystal nucleus migrates toward the nucleus, promoting the growth of the metallic iron grains. After 60 minutes of reduction, the grain growth is in a stable stage when small grain iron migrates to form larger-size grains. With a large specific surface area and low surface activity, the maximum size of the iron particles is about 120  $\mu\text{m}$ . Meanwhile, due to the

development of crystal lattice, the grains are uniformly aggregated and the lattice defects are reduced. Thus, the structure tends to be stable.

The cumulative percentage of metallic iron particles when the nickel slag is reduced at 1473 K for different durations is shown in Figure 8. With the same reduction temperature, the size of the iron particles increases significantly with prolonged reaction time. When the reduction time is increased from 10 to 30 minutes, the maximum size of metallic iron particles increases from 13 to 48  $\mu\text{m}$ . When the reduction time is 40 minutes, the maximum size of iron particles reaches 96  $\mu\text{m}$ . When the reduction is extended from 50 to 60 minutes, the maximum size of iron particles increases from 115 to



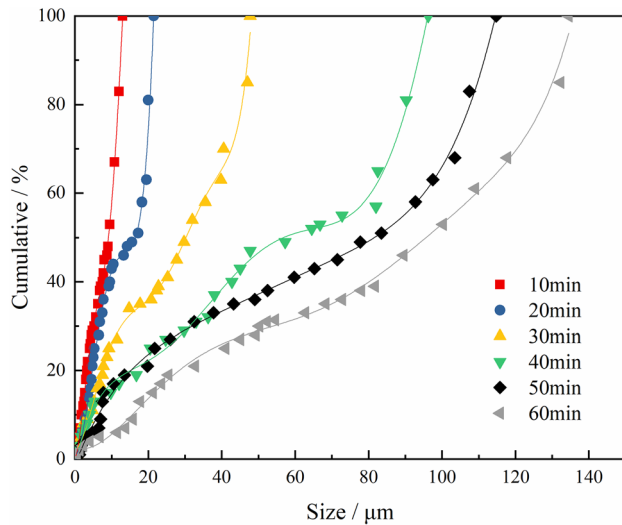


Fig. 8—Cumulative percentage of metallic iron particle size of the nickel slag reduced at 1473 K for different durations.

135  $\mu\text{m}$ . It can be speculated that if the reduction is further increased, the agglomeration of the iron particles will be greater. This is because the growth of iron particles is a process of diffusion and aggregation of metallic iron, and prolonging the reaction time is advantageous for the aggregation and growth of iron particles.

### 2. Effect of temperature on iron particle size distribution

Temperature is a decisive factor affecting the growth of iron particles. As temperature increases, the diffusion and migration speed of iron increases, which is beneficial to the diffusion and solidification of the metallic iron phase. The morphology of the reduction product of nickel slag at different temperatures for 60 minutes is shown in Figure 9. As the reduction temperature rises from 1370 K to 1423 K, the metallic iron particles increase dramatically. With the further rise of reduction temperature to 1473 K and 1523 K, the number of metallic iron particles decreases while the particle size is increased significantly. It can be speculated that if the reaction temperature is further increased, the metallic iron particles will further aggregate toward the center and grow.

The cumulative percentage of metallic iron particle size when the nickel slag is reduced for 60 minutes at different temperatures is shown in Figure 10. When the reduction temperature rises from 1373 K to 1523 K, the maximum size of the metallic iron particles increases from 21 to 170  $\mu\text{m}$ . From the thermodynamic perspective of iron particle nucleation, as the temperature increases, the Gibbs free energy of the reaction becomes more and more negative, which is conducive to the nucleation of metallic iron particles.<sup>[15]</sup> From a kinetic point of view, increasing the reduction temperature can improve the diffusion and migration ability of the

metallic iron particles, in which the latter has a profound influence on the size of the metallic iron particles. The relationship between the particle diffusion coefficient  $D$  and the temperature  $T$ <sup>[18]</sup> is as follows:

$$D = D_0 \exp\left(-\frac{Q_D}{kT}\right), \quad [11]$$

where  $Q_D$  is the diffusion activation energy. When the temperature is low, the metallic iron particles are in the early stage of structure formation. Due to the weak particle diffusion ability, it is difficult for the particles to form and grow, hence the small size of metallic iron particles. With the rise of reduction temperature, the particle diffusion capacity increases. At the boundary of fine iron particles, there is large crystal surface energy, which is the most important driving force for particle growth. As it becomes larger, it further pushes the mass points inside the particle to spread beyond the boundary to large neighboring particles, causing grain boundary to move and thus the particles grow. Therefore, in the growth process of the metallic iron particles from coal-based direct reduction of the nickel slag, the small-size iron particles grow bigger gradually and become fewer and fewer, while there are more and more large-size iron particles.

### 3. Effect of basicity on iron particle size distribution

The nickel slag is reduced for 60 minutes at 1473 K, and the effect of basicity on the growth of iron particles is shown in Figure 11. As shown in Figures 11(a) through (c), the size of the iron particles in the reduction product with a higher basicity is significantly larger than that of the iron particles in the product with a lower basicity. This is because under the condition of high basicity, the reaction of  $\text{Fe}_2\text{SiO}_4$  with  $\text{CaO}$  in the nickel slag causes the  $\text{FeO}$  to be displaced and dissociated, and the reduction of iron becomes easy. However, when the basicity is increased to 1.2, the maximum size of the metallic iron particles decreases (as shown in Figure 11(d)). The reason is that the high basicity increases the unreacted high melting point  $\text{CaO}$ , and  $\text{CaSiO}_3$  with a high melting point increases the melting point of the slag phase, making the diffusion of the iron phase in solid medium difficult. Meanwhile, the rise in slag increases the distance between the iron phases, which is detrimental to the diffusion and aggregation of the iron phases, so the reduction reaction is inhibited. Therefore, under the condition of the same reaction temperature and time, appropriate basicity is conducive to the agglomeration of iron in the reduction process, but excessive basicity can inhibit the agglomeration of iron in the reduction process.

The cumulative size distribution of the metallic iron particles at different basicity is shown in Figure 12. When the basicity is 0.6, 0.8, 1.0, and 1.2, the maximum size of the iron particles is 99, 135, 173, and 29  $\mu\text{m}$ , respectively. The appropriate basicity is 1.0 under experimental conditions.

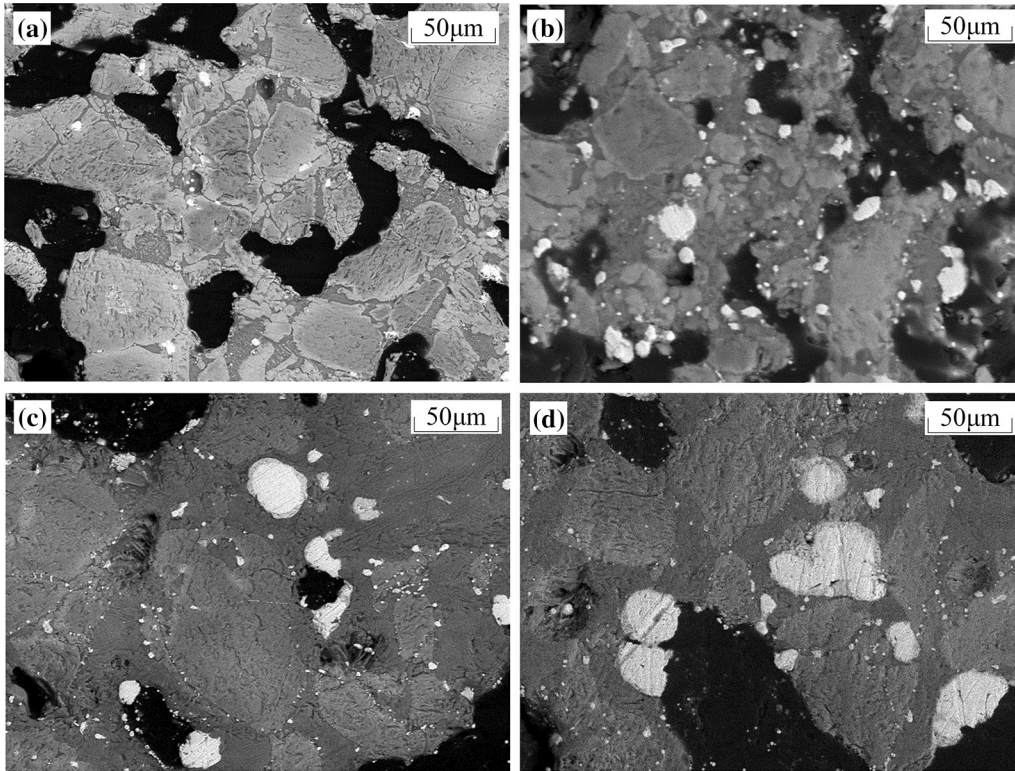


Fig. 9—Scanning electron micrographs of the nickel slag reduced at (a) 1373 K, (b) 1423 K, (c) 1473 K and (d) 1523 K for 60 min.

#### D. Growth Kinetics of Metallic Iron Particles

The growth kinetics of metallic particles in the reduction product of nickel slag can be described by the following classical kinetic equation.<sup>[19,20]</sup>

$$D^{1/n} - D_0^{1/n} = K \cdot t, \quad [12]$$

where  $D$  ( $\mu\text{m}$ ) is the particle size at time  $t$ ,  $D_0$  ( $\mu\text{m}$ ) is the initial particle diameter at  $t = 0$ ,  $n$  is the kinetic energy growth index of particles and is dimensionless,  $K$  is a temperature-dependent constant, which is dimensionless, and  $t$  is the growth time (min).

Parameter  $K$  satisfies the Arrhenius relationship shown in Eq. [8].

$$K = K_0 \exp\left(-\frac{Q}{RT}\right), \quad [13]$$

where  $K_0$  is the pre-exponential factor, which is dimensionless,  $Q$  is the particle growth activation energy ( $\text{kJ mol}^{-1}$ ),  $R$  is the gas constant ( $\text{J mol}^{-1} \text{K}^{-1}$ ), and  $T$  is the absolute temperature (K).

Substituting Eq. [7] into Eq. [8], we have

$$D^{1/n} - D_0^{1/n} = t \cdot K_0 \exp\left(-\frac{Q}{RT}\right) \quad [14]$$

Since no metallic iron particles have been generated at  $t = 0$ , Eq. [9] can be expressed as

$$D^{1/n} = t \cdot K_0 \exp\left(-\frac{Q}{RT}\right) \quad [15]$$

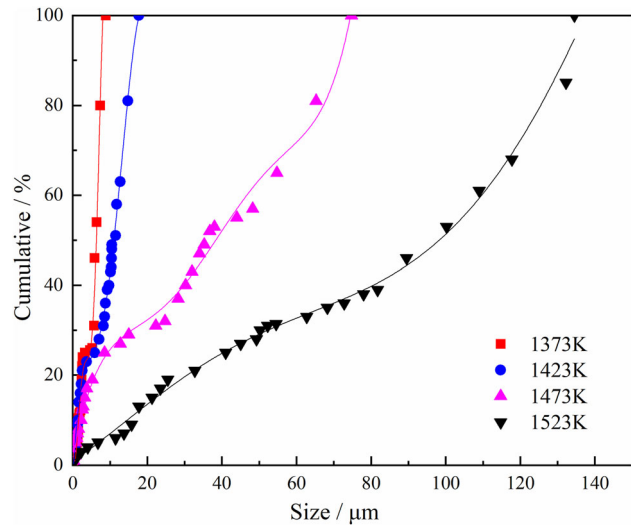


Fig. 10—Cumulative percentage of metallic iron particle size of the nickel slag reduced for 60 min at different temperatures.

Take the logarithm of both sides, and we obtain the following equation:

$$\ln D = n \ln t + n \ln K_0 - n \cdot \frac{Q}{RT} \quad [16]$$

As can be seen from the above equation, the values of  $n$  and  $K$  can be obtained from the image slopes of  $\ln D$  vs  $\ln t$ , and  $D^{1/n}$  vs  $t$ , respectively. Given  $n$  and  $K$ , the values of  $Q$  and  $K_0$  can be obtained from the slope and



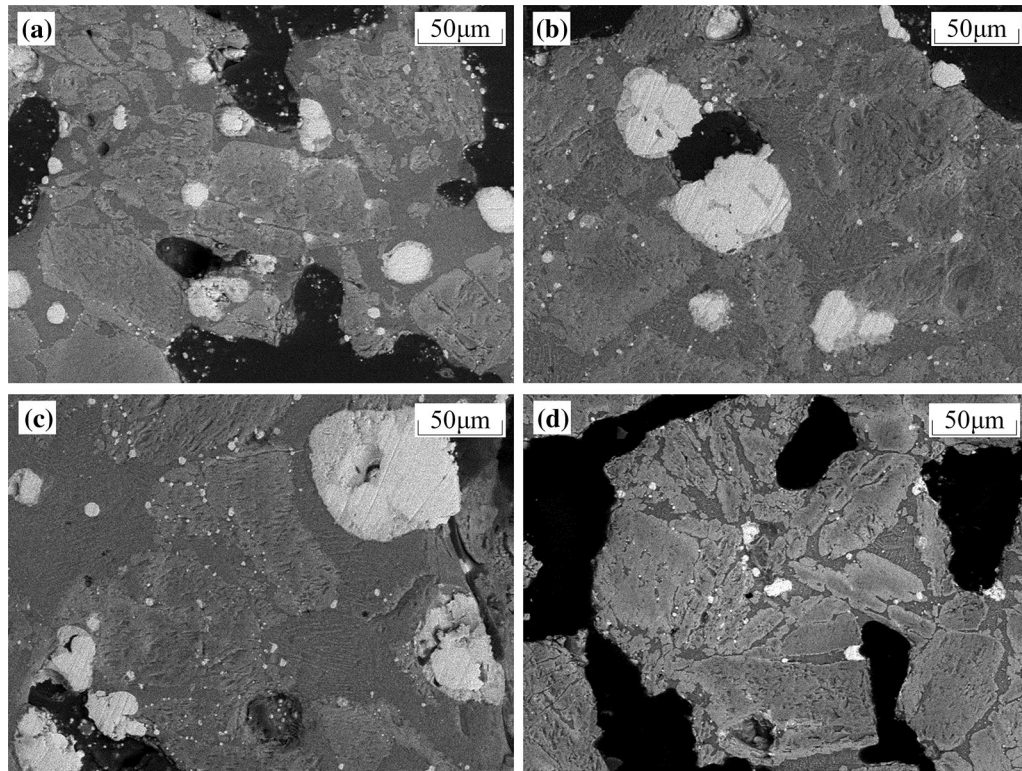


Fig. 11—Scanning electron micrographs of the nickel slag at basicity (a) 0.6, (b) 0.8, (c) 1.0, (d) 1.2 reduced at 1473 K for 60 min.

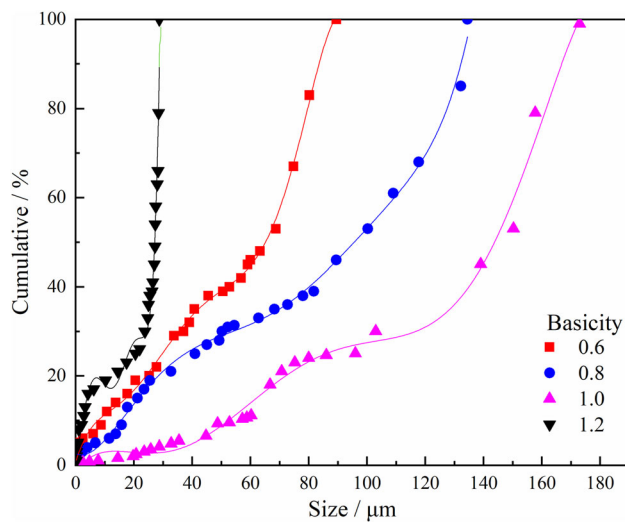


Fig. 12—Cumulative percentage of metallic iron particle size after the reduction of nickel slag with different basicity.

intercept of  $\ln K$  vs  $T^{-1}$  images, respectively. After the values of  $n$ ,  $K_0$ , and  $Q$  are determined from the experimental data, a growth model of metallic iron particles can be established.

The relationship between  $\ln D$  and  $\ln t$  of iron particles in the nickel slag product drawn from experimental data is shown in Figure 13. The straight line does not show good linear correlation at different temperatures.

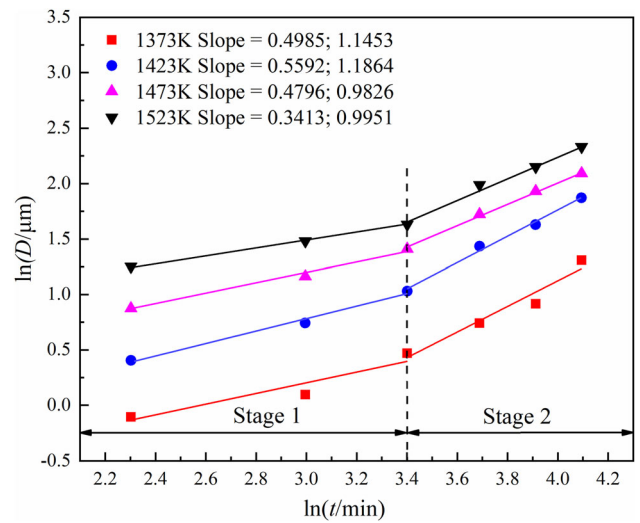
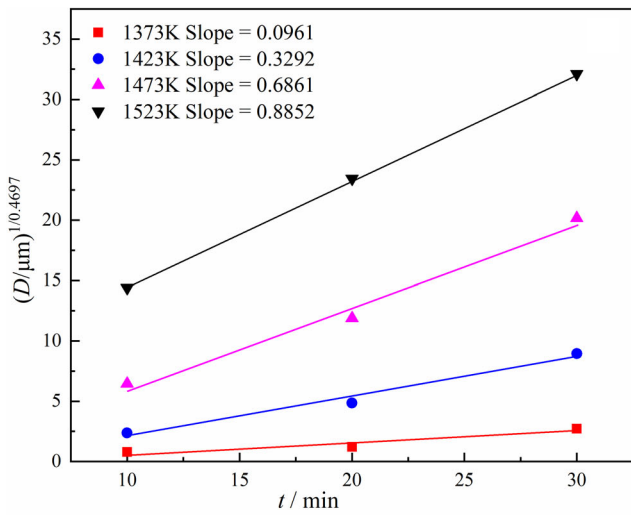
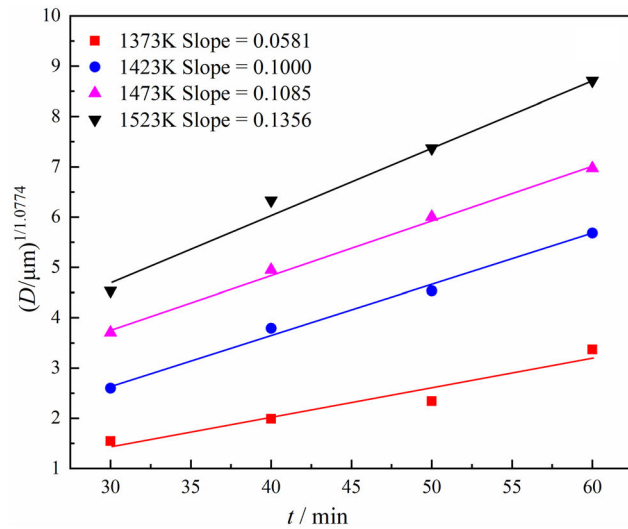


Fig. 13—Relationship between  $\ln D$  and  $\ln t$  of iron particles in the nickel slag at different temperatures.

Therefore, the entire reduction process is divided into two stages with 30min as the cut-off point for analysis. The two stages have an  $n$  value of 0.4697 and 1.0774, respectively, which represent different metal particle growth mechanisms.<sup>[21,22]</sup> The constant change of  $n$  value indicates that the coal-based reduction of nickel slag is a very complicated process.



(a)



(b)

Fig. 14—Relationship between  $D^{1/n}$  and  $t$  of iron particles in the nickel slag at different temperatures during (a) Stage 1, (b) Stage 2.

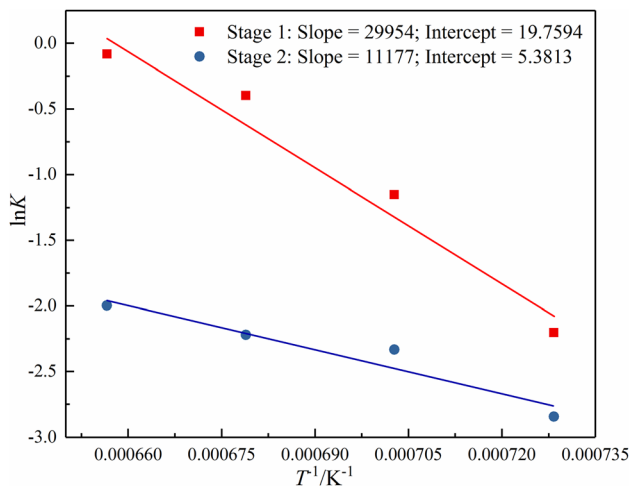


Fig. 15—Relationship between  $\ln K$  and  $T^{-1}$  of iron particles in the nickel slag.

Figure 14 shows the linear relationship between  $D^{1/n}$  and  $t$  at different temperatures. Figure 14(a) is the reduction process from 10 to 30 minutes, and Figure 14(b) is the reduction process from 30 to 60 minutes. The correlation coefficient  $K$  is obtained from the slope of the line in the graph.

Figure 15 shows the relationship between  $\ln K$  and  $T^{-1}$  at different temperatures in Stage 1 and 2. Stage 2 has better linear correlation than Stage 1. This is because in the initial stage of reaction, the reduction process is just beginning, and the growth of metallic iron particles is affected by the grain boundary diffusion and the reduction reaction of the iron oxide. As time passes

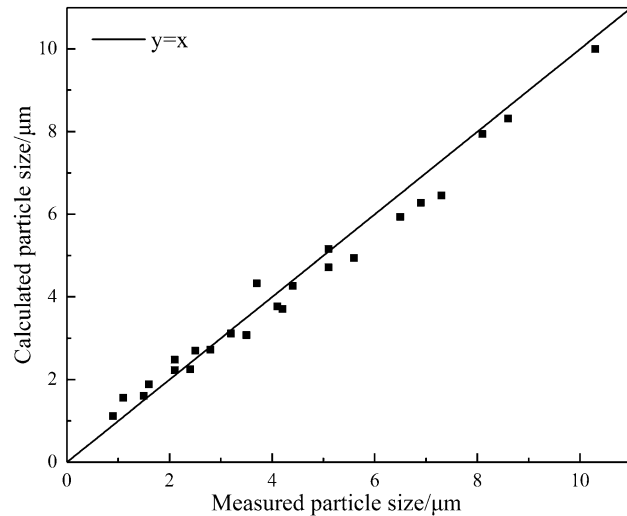


Fig. 16—Linear correlation of the growth model of metallic iron particles in the reduction process of nickel slag.

and temperature increases, the control factors of metallic iron particle growth are surface diffusion and particle migration. The growth of iron particle tends to be stable and the relationship between  $\ln K$  and  $T^{-1}$  approximately keeps a linear relationship.

The values of  $Q$  and  $K_0$  in the two stages can be obtained from the slope and intercept of the two straight lines in the figure. In Stage 1,  $Q$  is  $249.04 \text{ kJ mol}^{-1}$  and  $K_0$  is  $3.81 \times 10^8$ , while in Stage 2  $Q$  is  $92.93 \text{ kJ mol}^{-1}$  and  $K_0$  is 217.30. Therefore, the growth model of metallic iron particles in the direct reduction process of nickel slag can be expressed as

Stage 1 :

$$D^{1/0.4697} = 3.81 \times 10^8 t \cdot \exp\left(-\frac{249.04 \times 10^3}{RT}\right) \quad [17]$$

$$\text{Stage 2 : } D^{1/1.0774} = 217.3t \cdot \exp\left(-\frac{92.93 \times 10^3}{RT}\right) \quad [18]$$

The formation and growth of metallic iron particles is a process of nucleation and growth of the crystal. According to the theory of crystal growth, the solute supersaturation concentration is considered as the main driving force of grain growth. The activation energy  $Q$  in the metallic iron particle growth model varies with the particle growth index  $n$ . The content of metallic iron in Stage 1 is lower than that in Stage 2, which makes the driving force of grain growth in Stage 2 greater. The diffusion of metallic iron in the porous heterogeneous phase is more difficult than that in the homogeneous phase, so the growth of metallic iron particles in Stage 2 is easier and its activation energy  $Q$  is lower.

#### E. Correlation Analysis of the Growth Model

The comparison between the measured size and the calculated size of metallic iron particles in the direct coal-based reduction process of nickel slag is shown in Figure 16. The straight line is  $y = x$ , and the two sets of data are evenly distributed around the straight line, which indicates that the established growth model has good correlation. Therefore, the model can be used to describe the growth size of iron particles in the direct reduction process of nickel slag.

## IV. CONCLUSION

- (1) The direct reduction method can extract metallic iron from the nickel slag effectively. When the reduction temperature is 1573 K and the reduction time is 60 minutes, the degree of metallization of the product can reach 91.89 pct.
- (2) Large quantities of metallic iron particles are produced in the direct reduction process of nickel slag. Temperature and time are the main factors affecting the growth of iron particles. Prolonged reduction time is conducive to the aggregation and growth of the iron particles, and the increase of temperature is beneficial to the reduction reaction and the diffusion and aggregation of the iron phase. When the reduction temperature is 1373 K and the reduction time is increased from 10 to 60 minutes, the average size of the iron particles increases from 0.9 to 3.7  $\mu\text{m}$ . When the reduction temperature is 1523 K, the average size of the iron particles increases from 3.5 to 10.3  $\mu\text{m}$ .
- (3) During the direct reduction process of nickel slag, the metallic iron particles gradually aggregate and grow by the principle of minimum free energy, and

become spherical particles embedded in the slag phase. According to the changing trend of particle size, the direct reduction process can be divided into two stages: growth stage and stabilization stage. Their kinetic models are as follows:  $D^{1/0.4697} = 3.81 \times 10^8 t \cdot \exp\left(-\frac{249.04 \times 10^3}{RT}\right)$  (10 minutes  $\leq t \leq 30$  minutes, 1373 K  $\leq T \leq 1523$  K);  $D^{1/1.0774} = 217.3t \cdot \exp\left(-\frac{92.93 \times 10^3}{RT}\right)$  (30 minutes  $\leq t \leq 60$  minutes, 1373 K  $\leq T \leq 1523$  K). There is good correlation between the measured size and the calculated size of metallic iron particles.

## ACKNOWLEDGMENT

We thank the National Natural Science Foundation of China (No. 51774224) for financial support for this research.

## CONFLICT OF INTEREST

There is no conflict of interest.

## REFERENCES

1. YS Sun, Q Zhang, YX Han, P Gao, and GF Li: *JOM*, 2018, vol. 70, pp. 144–49.
2. C Cheng, QG Xue, G Wang, YY Zhang, and JS Wang: *Metall. Mater. Trans. B*, 2016, vol. 47B, pp. 154–63.
3. N Peng, B Peng, LY Chai, M Li, JM Wang, H Yan, and Y Yuan: *Miner. Eng.*, 2012, vol. 35, pp. 57–60.
4. YS Sun, YX Han, P Gao, ZH Wang, and DZ Ren: *Int. J. Miner. Metall. Mater.*, 2013, vol. 20, pp. 411–19.
5. CF Zhang, HX Liu, and DL Zhong: *Chin. J. Nonferrous Met.*, 1999, vol. 9, pp. 805–10.
6. S Wang, W Ni, KQ Li, CL Wang, and JY Wang: *Trans. Mater. Heat Treat.*, 2014, vol. 35, pp. 23–28.
7. S Wang, W Ni, KQ Li, CL Wang, and JY Wang: *Trans. Mater. Heat Treat.*, 2015, vol. 36, pp. 7–12.
8. P Gao, YS Sun, DZ Ren, and YX Han: *Miner. Metall. Process.*, 2013, vol. 30, pp. 74–78.
9. DQ Zhu, YZ Xiao, TJ Chun, and J Pan: *Chin. J. Nonferrous Met.*, 2013, vol. 23, pp. 3242–47.
10. J Pan, GL Zhang, DQ Zhu, and XL Zhou: *Trans. Nonferrous Met. Soc. China*, 2013, vol. 23, pp. 3421–27.
11. YG Guo, R Zhu, ZY Pei, MS Ma, Y Wang, and J Liu: *China Nonferrous Metall.*, 2017, vol. 10, pp. 75–80.
12. J Luo, GH Li, ZW Peng, MJ Rao, YB Zhang, and T Jiang: *JOM*, 2016, vol. 68, pp. 3015–21.
13. P Gao, YX Han, YJ Li, and YS Sun: *J. Northeast. Univ. Nat. Sci.*, 2012, vol. 33, pp. 133–36.
14. MS Chu, ZG Liu, ZC Wang, KJ Wu, and JP Lv: *China Metall.*, 2011, vol. 21, p. 17.
15. DQ Zhu, TJ Chun, and J Pan: *J. Univ. Sci. Technol. Beijing*, 2011, vol. 33, pp. 1325–30.
16. HZ Liu, WB Hu, MY Gu, and RJ Wu: *J. Inorg. Mater.*, 2002, vol. 33, pp. 430–35.
17. HD Wang, H Zhang, HL Li, and YC Tang: *Chin. J. Nonferrous Met.*, 2007, vol. 17, pp. 991–95.
18. XP Zhang and SL Liu: *J. Northeast Univ. Technol.*, 1993, vol. 14, pp. 28–31.



19. F.A. Nichols, *J. Appl. Phys.*: 1966, vol. 37, pp. 4599-02.
20. GS Li, LP Li, BG Juliana, and BF Woodfield: *J. Am. Chem. Soc.*, 2005, vol. 127, pp. 8659–66.
21. AJ Song, MZ Ma, RZ Zhou, L Wang, WG Zhang, CL Tan, and RP Liu: *Mater. Sci. Eng.*, 2012, vol. 538, pp. 219–23.

22. R Chaim: *Mater. Sci. Eng.*, 2007, vol. 443, pp. 25–32.

**Publisher's Note** Springer Nature remains neutral with regard to jurisdictional claims in published maps and institutional affiliations.